PARAMETER-FREE AUTOMATED EXTRACTION OF NEURONAL SIGNALS FROM CALCIUM IMAGING DATA

Yuri Levin-Schwartz[1], *Dennis R. Sparta*[2], *Joseph F. Cheer*[2,3], *and Tülay Adalı*[1]

[1]Department of Computer Science and Electrical Engineering, University of Maryland, Baltimore County
[2]Department of Anatomy and Neurobiology, University of Maryland, School of Medicine
[3]Department of Psychiatry, University of Maryland, School of Medicine

ABSTRACT

The use of *in vivo* calcium imaging has granted researchers the unprecedented ability to study large populations of neurons in real time, enabling direct observation of how the brain processes information. Such data offers great potential, however for current analysis techniques, successful extraction of the true neuronal signals is intimately tied to the proper selection of multiple user-defined parameters, which must be tuned for each video sequence. To overcome such issues, we propose a novel parameter-free independent component analysis (ICA)-based method, ICA with signal reconstruction and ordering (ICA+SRO), to automatically extract neuronal signals from calcium imaging sequences. The power of ICA+SRO is demonstrated on a real calcium imaging sequence. We compare the results of ICA+SRO with those from the popular principal component analysis-ICA based technique and show significant improvement. The results demonstrate the simplicity of a parameter-free method and its power in extracting neuronal signals from calcium imaging sequences.

Index Terms— Independent Component Analysis, Calcium Imaging, Data-Driven Analysis

1. INTRODUCTION

A fundamental goal in modern neuroscience research is understanding how behavior is encoded by the brain. This goal has been greatly forwarded by very recent advances in imaging technology, see $e.g.$, [2,22], which have enabled the study large populations of neurons in real time. Given the potential offered by such imaging data, many methods have been developed to extract individual neuronal signals from the high levels of noise in the fluorescence images.

Traditional analysis of calcium imaging data is based on manual selection of regions of interest (ROI), see $e.g.$, [3, 5, 10, 16, 18]. However, ROI-based analyses are subjective, since they are based almost entirely on human intuition and can be quite labor intensive when the number of neurons is in the hundreds. More recently, automated methods for the extraction of neuronal signals from calcium imaging sequences have been developed, see $e.g.$, [19, 21]. These methods are generally based on the assumption that the spatio-temporal neuronal signals can be factored into a product of two matrices, one that encodes the spatial location of each neuron and one that describes the temporal evolution of calcium concentration for each neuron [13]. Many methods have been developed based on this assumption, including those based on principal component analysis (PCA) and independent component analysis (ICA) [9, 12], dictionary learning [11], graph cut-related algorithms [4], nonnegative matrix factorization [8], and constrained non-negative matrix factorization [13]. However, while potentially powerful, the success of these methods is intimately tied to the proper selection of multiple user-defined parameters, which must be appropriately tuned for each video sequence.

In this paper, we propose a fully automated and completely parameter-free technique, ICA with signal reconstruction and ordering (ICA+SRO), for the extraction of neuronal spatial locations and their calcium concentrations over time. We apply ICA+SRO to real *in vivo* calcium imaging data from the brains of freely moving mice in fairly high noise levels and compare its performance with that of the popular PCA-ICA method proposed in [9].

2. MATERIAL AND METHODS

2.1. Background

2.1.1. PCA

Let the calcium imaging sequence be represented by $\mathbf{X} \in \mathbb{R}^{T \times P}$, where T is the number of frames in the video sequence and P is the number of pixels in each florescence image. Since the number of neurons is usually much lower than T, dimension reduction is a crucial preprocessing step in order to remove noise and avoid overfitting. Thus prior to processing the video, dimension reduction is performed using

*The work of Y. Levin-Schwartz and T. Adalı was supported by the following grant NSF-CCF 1618551. The work of J. F. Cheer was supported by NIH grants DA022340 and DA042595.

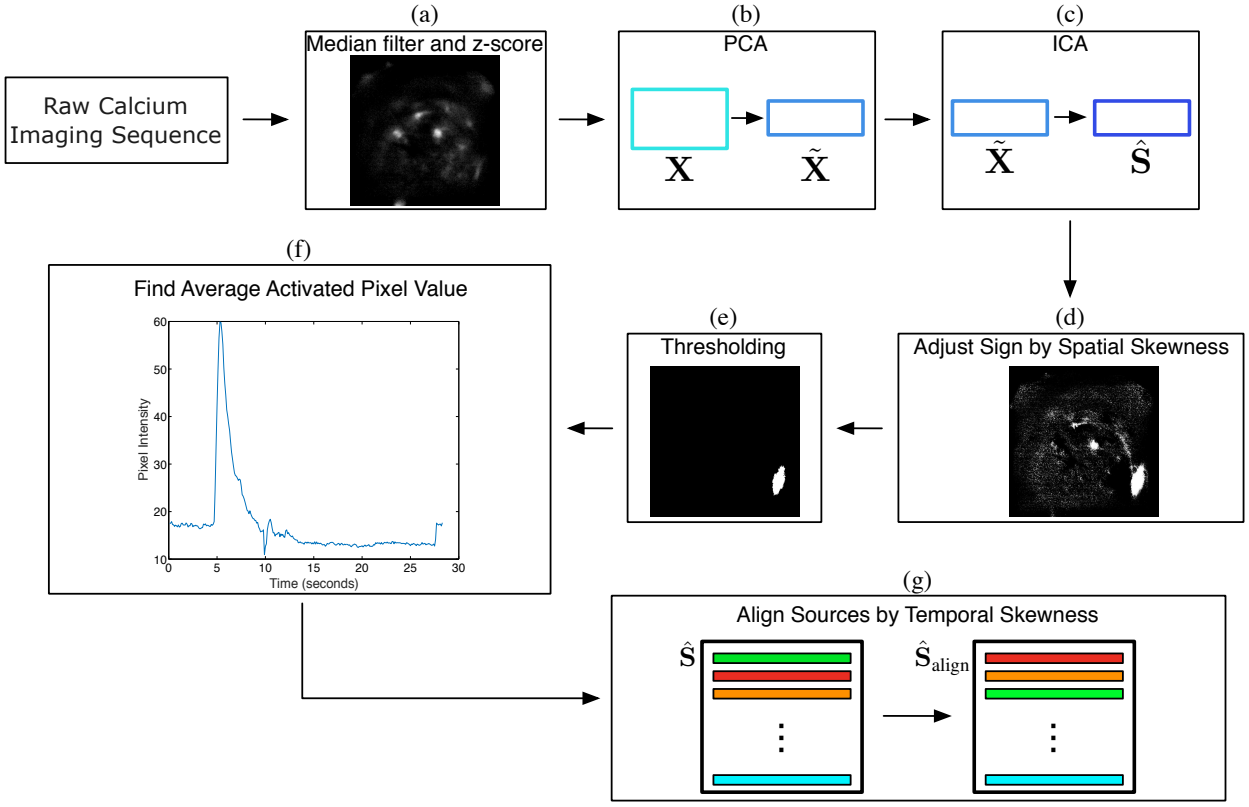

Fig. 1. Illustration of the proposed calcium imaging framework, ICA+SRO. The pipeline is as follows: (a) the raw calcium imaging sequnce is median filtered and z-scored, then (b) dimension reduction using PCA is performed and (c) ICA is run. (d) the sign of each component is adjusted according to the sign of the each component's spatial skewness and (e) the components are thresholded. (f) the average pixel value withing each thresholded image is found for each time, then (g) the components are aligned according to the skewness of their time courses.

PCA, with the order specified by K, in order to reduce $\mathbf{X}$ to $\tilde{\mathbf{X}} \in \mathbb{R}^{K \times P}$, such that

$$\tilde{\mathbf{X}} = \mathbf{F}\mathbf{X}, \tag{1}$$

where $\mathbf{F} \in \mathbb{R}^{T \times K}$ is the data reduction matrix and is equal to the eigenvectors corresponding to the highest K eigenvalues of the sample covariance matrix of $\mathbf{X}$. There are many methods that can be used to estimate K, see $e.g.$, [17, 20], however most classical methods ignore important properties of the signals, such as sample-to-sample dependence, which can lead to an over estimation of K. In this work, we use the new order-selection method described in [7], due to its high performance on real functional magnetic resonance imaging data, which exhibit similar sample-to-sample dependence as that seen in calcium imaging data. The method employs an iterative procedure to jointly estimate a downsampling depth, producing samples with effectively no sample-to-sample dependence, and a model order, both through the use of the minimum description length [14] (Bayesian information criterion [15]).

2.1.2. ICA

Following PCA, $\mathbf{X}$ is transformed into $\tilde{\mathbf{X}} \in \mathbb{R}^{K \times P}$, which contains the mixed neuronal signals. Note that through the use of PCA, we have removed the contribution of the $(T - K)-$dimensional noise subspace of $\mathbf{X}$ and are left with the $K-$dimensional signal subspace; therefore the noiseless ICA model can be seen as a natural match to the underlying problem. The noiseless ICA model for $\tilde{\mathbf{X}}$ is given by

$$\tilde{\mathbf{X}} = \tilde{\mathbf{A}}\mathbf{S}, \tag{2}$$

where the K latent sources in $\mathbf{S} \in \mathbb{R}^{K \times P}$ are mixed by an invertible mixing matrix $\tilde{\mathbf{A}} \in \mathbb{R}^{K \times K}$. Through the assumption of statistical independence on the part of sources, ICA seeks to estimate a demixing matrix, $\mathbf{W} \in \mathbb{R}^{K \times K}$, such that the estimated components are given by $\hat{\mathbf{S}} = \mathbf{W}\mathbf{X}$. The estimated temporal evolution of each component in $\hat{\mathbf{S}}$ or time courses, $\hat{\mathbf{A}}$, are given by

$$\hat{\mathbf{A}} = \mathbf{F}^{\mathrm{T}}\tilde{\mathbf{A}}, \tag{3}$$

where $(\cdot)^{\mathrm{T}}$ denotes the matrix transpose. Reliable extraction of the latent sources, up to scaling and permutation ambigu-

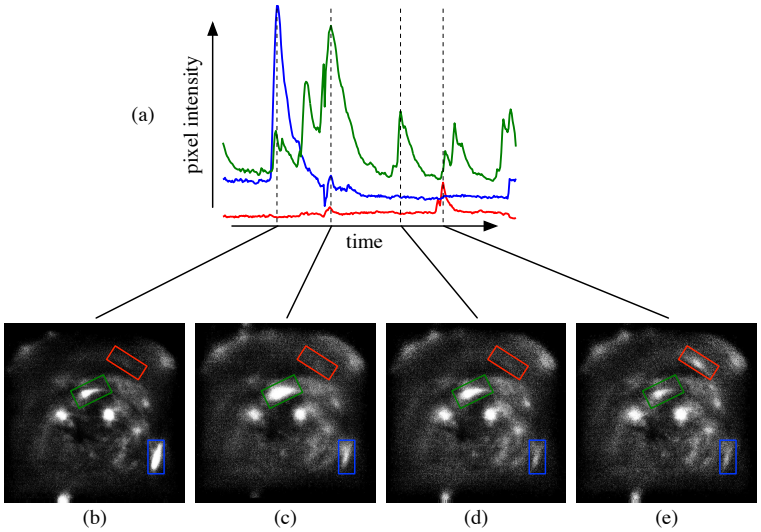

Fig. 2. Timecourses for the detected neurons (a) and selected frames from the analyzed calcium imaging sequence (b)-(e). The color of the timecourse in (a) corresponds to the color of the box in the frames. Note that ICA+SRO can detect both faint and strong neuronal activity identified using a red box and green box, respectively.

ities, is dependent upon accurately modeling their distributions, since improper modeling will lead to poor ICA performance when the true sources vary greatly from the assumed distribution [1]. For this reason, we use the parameter-free entropy bound minimization (EBM) [6] as the ICA algorithm in this work, since it can describe a wide variety of distributions including those that are unimodal, bimodal, symmetric, and skewed. Skewed distributions are a good match for the neuronal spatial locations due to the fact that they can reasonably be expected to be small relative to the total size of the image and have a higher intensity than the background.

2.2. ICA+SRO

The calcium imaging framework, ICA+SRO, depicted in Figure 1 seeks to decompose the raw calcium imaging sequence into a set of spatial neuronal footprints and their corresponding timecourses. In the first stage, we preprocess the data and perform ICA. The first stage begins by applying a median filter and z-scoring each image in the sequence in order to remove the majority of the high frequency noise. Next, PCA is performed according to (1), with the order, 15 for this video, specified using the method in [7]. Then, ICA using the EBM algorithm is performed on $\tilde{\mathbf{X}}$, producing $\hat{\mathbf{S}}$.

In the second stage, we analyze the estimated components in order to determine the true neuronal spatial locations and corresponding timecourses. The first step is to resolve the sign ambiguity of ICA. This is accomplished by examining the skewness, a measure of a distribution's asymmetry about its mean, of each estimated component. The skewness of a random variable, y, is defined as

$$\gamma = \frac{\mathrm{E}\left[(y-\mu)^3\right]}{\left(\mathrm{E}\left[(y-\mu)^2\right]\right)^{3/2}},$$

where $\mathrm{E}(\cdot)$ is the expected value operator and μ is the mean of y, thus if the tail of the distribution of y is larger on the right of μ than on the left, the skewness will be positive. Since the neuronal footprint should be small relative to the size of the image and have a higher intensity value than the background, its spatial skewness should be positive. Thus, we compute the skewness of each estimated component and invert the image and its corresponding time course if the skewness is negative. As can be seen in Figure 1d, though the spatial neuronal footprint is the largest object in the estimated component, the component contains some noise. For this reason, after adjusting the sign of each component, we threshold the images, selecting only those pixels that are pure white, $i.e.$, have maximum intensity, and find the largest object that survives the threshold. The resulting component, if it describes true neuronal activation, will contain only the spatial footprint of the neurons. We should note that since ICA naturally takes the temporal evolution of the components into account through its mixing model, if a component is related to true neuronal activation, the largest object in that component must be the spatial footprint of the neuron. Once the largest object in each component is selected, for each component, we compute the average pixel intensity of the thresholded object for each frame, producing the final timecourse for that component. This step helps to remove the noise from the timecourses and removes the scaling ambiguity that is inherent in

	EBM	stICA, $\mu = 0$	stICA, $\mu = 0.1$	stICA, $\mu = 0.2$	stICA, $\mu = 0.3$
Proposed Framework	3	3	3*	3*	3*
Framework in [9]	2	2	2*	2*	2*

Table 1. Number of detected neurons found using ICA+SRO and the framework in [9] with different ICA algorithms. The correct number of neurons, assessed through visual inspection, is 3. The parameter μ for stICA controls the trade-off between spatial ICA and temporal ICA, with $\mu = 0$ being solely spatial ICA and $\mu = 1$ being solely temporal ICA. Entries that have $(\cdot)*$ are cases where one or more neurons is split between multiple components. ICA+SRO can find all 3 neurons and ICA-EBM does not split the neuronal signals. The performance of stICA is dependent on the choice of μ, with the optimal value for this data being 0.

ICA. In the final step, we order the components based upon the skewness of their timecourses. Since the amount of neuronal activity is, in general, sparse when compared to T, the skewness of the timecourse should be fairly high when compared to a component that is just noise. Thus, by ordering the components by their temporal skewness, we automatically sort the components from most likely to be true neuronal signals to those components that are least likely, thus simplifying any further studies.

2.3. Calcium Imaging Data

In order to record calcium activity in fully awake animals, GCaMP6.0, an ultrasensitive protein calcium sensor, is injected into the brain to transduce genetically identical neurons in heterogeneous brain tissue. Approximately four weeks after viral transduction, the animal is briefly anesthetized and a microendoscope is inserted into the same region using blood vessels as landmarks. After the desired field of view is obtained, a baseplate is fixed to the animal's head, thus making the endoscope more secure and limiting the potential for motion artifacts. Fluorescence images are obtained though implanted mini-endoscope using an integrated LED (473 nm). Images are acquired at 15 frames per second with the LED transmitting 0.1-0.2 mW of light on average. A total of 283 frames are collected, representing a time period of approximately 19 seconds.

3. RESULTS AND DISCUSSION

Figure 2 demonstrates the high level of accuracy achieved by ICA+SRO. The results match closely with a separate ROI analysis performed on the same sequence. Though not displayed here due to the space limitations, it should be noted that the three cells detected had the highest temporal skewness, thus showing the ability of the method to detect and separate neuronal signals from noise. In addition, as can be seen in Figure 2a, there is a clear drop in the intensity values for all three neurons shortly before the frame shown in Figure 2c. The reason for this is a major motion artifact, resulting from the fact that the data was gathered from a freely moving mouse. Such artifacts are not uncommon in such calcium imaging sequences and can cause problems for ROI-based analyses; however ICA+SRO had little trouble detecting the neuronal signals in spite of this.

We next compared ICA+SRO to the one proposed in [9], which is currently the most popular method for analyzing calcium imaging data. We also probed the effect of ICA algorithm choice by comparing the parameter-free EBM algorithm used in this work with the spatio-temporal ICA (stICA) algorithm in [9]. The stICA algorithm required user selection of a parameter μ, which controls the trade-off between spatial ICA and temporal ICA, with μ=1 being purely temporal ICA and μ=0 corresponding to purely spatial ICA. Note that the recommended value of μ in [9] between 0.1 and 0.2 . The results of the comparison are shown in Table 1.

From Table 1, we can see that irrespective of the ICA algorithm, the method proposed in [9] is unable to find all three neuronal signals. In contrast, ICA+SRO is able to detect all three neuronal signals, though when stICA is used instead of EBM, some neurons are split between multiple components for certain values of μ. We should note that the EBM algorithm did not split the neuronal signals among multiple components. This shows both the power of ICA+SRO and the importance of minimizing the number of parameters, as noted in the case of stICA, which heavily depends on the appropriate selection of μ, which is not a straightforward task. Also, note that the method proposed in [9] did not correctly sort the extracted components as our method does, requiring further manual processing to obtain the desired signals.

4. CONCLUSION

In this work, we developed a novel ICA-based method to identify and extract individual neuronal signals from calcium imaging data. This method circumvents a serious limitation of previous methods, which is the use of human intervention to isolate single neurons either through manual definition of ROI or appropriate determination of multiple user-specified parameters. Our proposed method, ICA+SRO, is parameter-free and automatically extracts and sorts neuronal signals. The power of ICA+SRO is demonstrated on a real calcium imaging sequence with both high noise and major motion artifacts and the results are significantly improved over those obtained using the popular framework proposed in [9]. The results show the power of our framework and its success without the need for manual selection of parameters, which can highly affect performance.

5. REFERENCES

[1] Jean-François Cardoso. Infomax and maximum likelihood for blind source separation. *IEEE Signal Process. Lett.*, 4(4):112–114, April 1997.

[2] Kunal K. Ghosh, Laurie D. Burns, Eric D. Cocker, Axel Nimmerjahn, Yaniv Ziv, Abbas El Gamal, and Mark J. Schnitzer. Miniaturized integration of a fluorescence microscope. *Nature Methods*, 8(10):871–878, 2011.

[3] Werner Göbel and Fritjof Helmchen. New angles on neuronal dendrites in vivo. *Journal of Neurophysiology*, 98(6):3770–3779, 2007.

[4] Patrick Kaifosh, Jeffrey D. Zaremba, Nathan B. Danielson, and Attila Losonczy. SIMA: Python software for analysis of dynamic fluorescence imaging data. *Frontiers in Neuroinformatics*, 8:1–10, 2014.

[5] Jason N. D. Kerr, David Greenberg, and Fritjof Helmchen. Imaging input and output of neocortical networks in vivo. *Proceedings of the National Academy of Sciences of the United States of America*, 102(39):14063–14068, 2005.

[6] Xi-Lin Li and Tülay Adalı. Independent component analysis by entropy bound minimization. *IEEE Transactions on Signal Processing*, 58(10):5151–5164, Dec. 2010.

[7] Xi-Lin Li, Sai Ma, V. D. Calhoun, and Tülay Adalı. Order detection for fMRI analysis: Joint estimation of downsampling depth and order by information theoretic criteria. In *IEEE Int. Symp. Biomedical Imaging: From Nano to Macro*, pages 1019–1022, April 2011.

[8] Ryuichi Maruyama, Kazuma Maeda, Hajime Moroda, Ichiro Kato, Masashi Inoue, Hiroyoshi Miyakawa, and Toru Aonishi. Detecting cells using non-negative matrix factorization on calcium imaging data. *Neural Networks*, 55:11–19, 2014.

[9] Eran A. Mukamel, Axel Nimmerjahn, and Mark J. Schnitzer. Automated analysis of cellular signals from large-scale calcium imaging data. *Neuron*, 63(6):747–760, 2009.

[10] Cristopher M. Niell and Stephen J. Smith. Functional imaging reveals rapid development of visual response properties in the zebrafish tectum. *Neuron*, 45(6):941–951, 2005.

[11] Marius Pachitariu, Adam M. Packer, Noah Pettit, Henry Dalgleish, Michael Hausser, and Maneesh Sahani. Extracting regions of interest from biological images with convolutional sparse block coding. In *Advances in Neural Information Processing Systems*, pages 1745–1753, 2013.

[12] Tapan P. Patel, Karen Man, Bonnie L. Firestein, and David F. Meaney. Automated quantification of neuronal networks and single-cell calcium dynamics using calcium imaging. *Journal of Neuroscience Methods*, 243:26–38, 2015.

[13] Eftychios A. Pnevmatikakis, Daniel Soudry, Yuanjun Gao, Timothy A. Machado, Josh Merel, David Pfau, Thomas Reardon, Yu Mu, Clay Lacefield, Weijian Yang, Misha Ahrens, Randy Bruno, Thomas M. Jessell, Darcy S. Peterka, Rafael Yuste, and Liam Paninski. Simultaneous denoising, deconvolution, and demixing of calcium imaging data. *Neuron*, 89(2):285–299, 2016.

[14] Jorma Rissanen. Modeling by shortest data description. *Automatica*, 14:465–471, 1978.

[15] Gideon Schwarz. Estimating the dimension of a model. *Ann. Stat.*, 6:461–464, 1978.

[16] Olav Stetter, Demian Battaglia, Jordi Soriano, and Theo Geisel. Model-free reconstruction of excitatory neuronal connectivity from calcium imaging signals. *PLoS Comput. Biol.*, 8(8):1–16, 2012.

[17] Petre Stoica and Yngve Selen. Model-order selection: a review of information criterion rules. *IEEE Signal Processing Magazine*, 21(4):36–47, July 2004.

[18] Elisenda Tibau, Miguel Valencia, and Jordi Soriano. Identification of neuronal network properties from the spectral analysis of calcium imaging signals in neuronal cultures. *Frontiers in Neural Circuits*, 7(199):1–16, 2013.

[19] Jakub Tomek, Ondrej Novak, and Josef Syka. Two-photon processor and SeNeCA: a freely available software package to process data from two-photon calcium imaging at speeds down to several milliseconds per frame. *Journal of Neurophysiology*, 110(1):243–256, 2013.

[20] Mati Wax and Thomas Kailath. Detection of signals by information theoretic criteria. *IEEE Trans. Acoust., Speech and Signal Process.*, 33(2):387–392, April 1985.

[21] Emre Yaksi and Rainer W Friedrich. Reconstruction of firing rate changes across neuronal populations by temporally deconvolved Ca2+ imaging. *Nature Methods*, 3(5):377–383, 2006.

[22] Yaniv Ziv and Kunal K. Ghosh. Miniature microscopes for large-scale imaging of neuronal activity in freely behaving rodents. *Current Opinion in Neurobiology*, 32:141–147, 2015.